Plasma Physics and Controlled Fusion

PAPER

Radial electric field and ion parallel flow in the quasi-symmetric and Mirror configurations of HSX

To cite this article: S T A Kumar *et al* 2018 *Plasma Phys. Control. Fusion* **60** 054012

View the article online for updates and enhancements.

Related content

- Determination of radial electric field from Pfirsch–Schlüter flows in the HSX stellarator
S.T.A. Kumar, J.N. Talmadge, T.J. Dobbins et al.
- Intrinsic plasma rotation and Reynolds stress at the plasma edge in the HSX stellarator
R.S. Wilcox, J.N. Talmadge, D.T. Anderson et al.
- Core density turbulence in the HSX Stellarator
C.B. Deng, D.L. Brower, D.T. Anderson et al.

Recent citations

- Stepped pressure equilibrium with relaxed flow and applications in reversed-field pinch plasmas
Z S Qu *et al*
- The role of neutral friction in governing parallel flows in the HSX stellarator
T.J. Dobbins *et al*
- Asymmetry of parallel flow on the Large Helical Device
J. Chen *et al*

IOP ebooks™

Bringing together innovative digital publishing with leading authors from the global scientific community.

Start exploring the collection–download the first chapter of every title for free.

This content was downloaded from IP address 144.92.31.246 on 30/06/2020 at 15:54

IOP Publishing Plasma Physics and Controlled Fusion
Plasma Phys. Control. Fusion **60** (2018) 054012 (6pp) https://doi.org/10.1088/1361-6587/aab4c7

Radial electric field and ion parallel flow in the quasi-symmetric and Mirror configurations of HSX

S T A Kumar[1], T J Dobbins[1], J N Talmadge[1], R S Wilcox[1,2] and D T Anderson[1]

[1] HSX Plasma Laboratory, Department of Electrical and Computer Engineering, University of Wisconsin-Madison, Madison, WI 53706, United States of America
[2] Oak Ridge National Laboratory, Oak Ridge, TN 37381, United States of America

E-mail: stkumar@wisc.edu

Received 19 December 2017, revised 14 February 2018
Accepted for publication 7 March 2018
Published 23 March 2018

Abstract

The radial electric field and the ion mean parallel flow are obtained in the helically symmetric experiment stellarator from toroidal flow measurements of C^{+6} ion at two locations on a flux surface, using the Pfirsch–Schlüter effect. Results from the standard quasi-helically symmetric magnetic configuration are compared with those from the Mirror configuration where the quasi-symmetry is deliberately degraded using auxiliary coils. For similar injected power, the quasi-symmetric configuration is observed to have significantly lower flows while the experimental observations from the Mirror geometry are in better agreement with neoclassical calculations. Indications are that the radial electric field near the core of the quasi-symmetric configuration may be governed by non-neoclassical processes.

Keywords: stellerator, radial electric field, flows

(Some figures may appear in colour only in the online journal)

1. Introduction

One of the salient features of plasma confined in a symmetric magnetic geometry is that it can exhibit large flows in the symmetry direction, like the toroidal rotation in tokamaks. Plasma flow in a conventional stellarator is damped both in the toroidal and poloidal directions due to the increased neoclassical viscosity arising from the large variations in the magnetic field strength. Due to the intrinsic non-ambipolarity of conventional stellarators, the radial electric field (E_r) and plasma flow are governed predominantly by neoclassical processes [1–3]. A quasi-symmetric stellarator has symmetry of $|\mathbf{B}|$ in the helical, axial or poloidal directions. It is an open question as to the extent that a deviation from perfect symmetry impacts whether neoclassical processes determine E_r and the plasma flow [4, 5].

The helically symmetric experiment (HSX) [6] is uniquely suited for investigating the effect of symmetry on flows and electric fields. HSX is optimized to reduce neoclassical transport by having a symmetry in the magnetic field strength in the helical direction. A set of 48 non-planar coils produce this quasi-helically symmetric (QHS) configuration with a single dominant spectral component with mode numbers $(n, m) = (4, 1)$, where n and m are toroidal and poloidal mode numbers respectively. Another set of 48 planar coils can be used to degrade this quasi-helical symmetry by introducing field variations in the toroidal direction with mode numbers $(n, m) = (4, 0)$ and $(8, 0)$ (called 'Mirror' configuration) [7]. The parallel neoclassical viscosity in the helical direction in the QHS configuration of HSX is calculated to be minimal compared to that in the Mirror configuration due to this quasi-symmetry. Experiments in the past, using a biased electrode at the edge to spin the plasma, have confirmed reduced flow damping [8] in the QHS geometry. In a separate experiment, it has been observed that the intrinsic parallel flow is predominantly in the quasi-symmetry direction in HSX [9]. Even though these two experiments demonstrated the neoclassical properties of QHS geometry in

 © 2018 IOP Publishing Ltd Printed in the UK

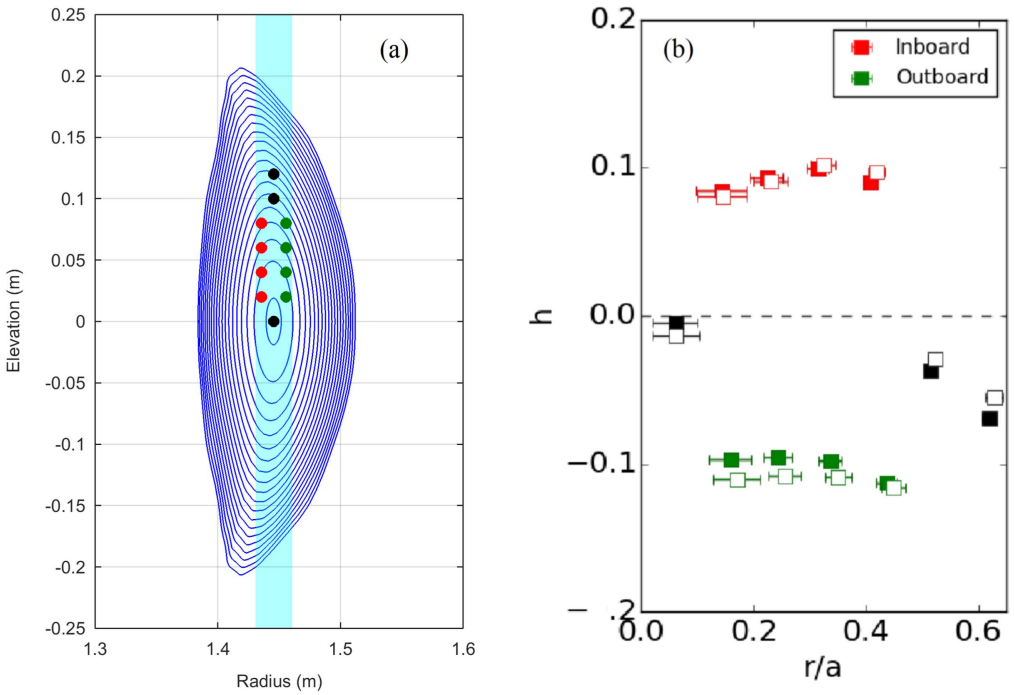

Figure 1. (a) Poloidal cross-section of HSX magnetic flux surfaces where the flow measurements are made. Vertical shaded band represents approximate $1/e$ width of the diagnostic hydrogen neutral beam. Red and green dots represent inboard and outboard measurement locations respectively. (b) The Pfirsch–Schlüter factor, h, calculated at the measurement locations for QHS (closed squares) and Mirror (open squares) geometries. A synthetic diagnostic model is used to obtain weighted average values along the sight-line-beam intersection. Horizontal 'error bars' represent the radial averaging.

terms of the direction of flows, the experimental values of the E_r and parallel flow do not agree with neoclassical calculations [9, 10]. This discrepancy is addressed in this paper in light of recent improvements in experimental techniques and measurements in both the QHS and Mirror configurations.

The rest of the paper is organized as follows: section 2 describes the experimental techniques. Experimental results for both configurations studied are given in section 3. Neoclassical calculations and comparison with experimental results are given in section 4. Discussions are detailed in section 5, followed by summary in section 6.

2. Experimental setup

Previously, the radial electric field was obtained in HSX using the radial force balance equation [9]. This method requires simultaneous and accurate measurements of poloidal and toroidal flows. In HSX, the poloidal flow measurements near the core have large uncertainties due to the relatively large width of the diagnostic neutral beam compared to the diameter of the flux surfaces. A poloidal sight-line cuts through many flux surfaces with varying flow vectors within the beam-sight-line intersection leading to a smeared measurement of the flow. In order to address this issue, a method has been developed to obtain the radial electric field and the mean parallel flow (referred to here as the 'bootstrap' flow) from parallel flows only, without using the radial force balance equation. This technique utilizes the fact that the Pfirsch–Schlüter flow ($v_{\rm PS}$) is directly proportional to the radial electric field through the relation,

$$v_{\rm PS} = hB\frac{{\rm d}\phi}{{\rm d}\psi} = v_{||i} - v_{\rm BS}, \qquad (1)$$

where ϕ is the electric potential, ψ is the toroidal flux, h is the Pfirsch–Schlüter geometric factor, $v_{||i}$ is the total ion parallel velocity at the measurement location, $v_{\rm BS}$ is the bootstrap portion of the flow and B is the toroidal magnetic field strength. As the ion temperature in HSX is low (∼50–60 eV) and the radial profile of ion temperature is nearly flat (see figures 2 and 4), the ion pressure gradient has been neglected. (The pressure gradient contribution to the Pfirsch–Schlüter flow is calculated to be less than the electric field contribution by a factor of ∼30.) It can be seen from equation (1) that the flux surface constants $\frac{{\rm d}\phi}{{\rm d}\psi}$ and $v_{\rm BS}$ can be obtained by measuring the parallel flow for at least two locations on a flux surface. Details of this measurement technique have been published elsewhere [10].

Localized parallel flows of C^{+6} ion for this experiment are obtained from the toroidal flows measured using charge exchange recombination spectroscopy (CHERS), accounting for the small angle the sight-line makes with the field line. The CHERS diagnostic in HSX uses a 30 keV, 4 Amp diagnostic hydrogen neutral beam to stimulate carbon impurity radiation. The CVI emission line at 529.1 nm is measured and spectrally resolved using a Czerny–Turner spectrometer. For the experiments reported in this paper, the viewing fiber assembly for the spectroscopy has been modified as shown in figure 1(a) to collect emission from the inboard and outboard locations near the core of the plasma. On-axis magnetic field

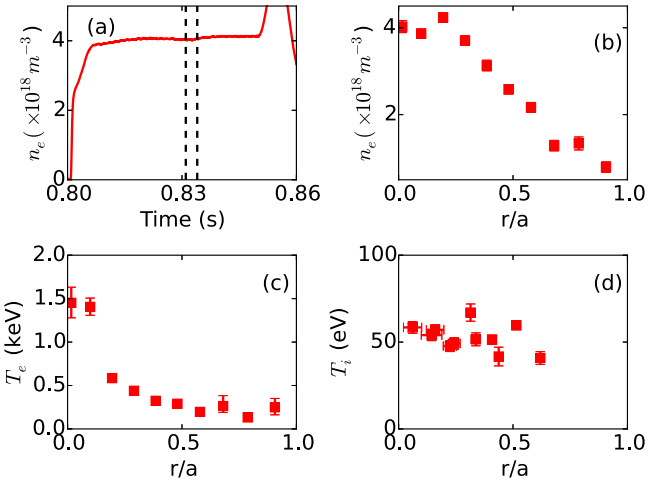

Figure 2. Discharge parameters for the QHS configurations. Line averaged electron density measured by an interferometer (a), radial profiles of electron density (b) and electron temperature (c) measured using Thomson scattering diagnostic at $t = 0.82$ s into the discharge, and C^{+6} ion temperature measured using CHERS (d). Vertical dashed lines on (a) represent start and end times of the diagnostic neutral beam. Data are averaged over 26 similar discharges used for the flow and E_r analysis.

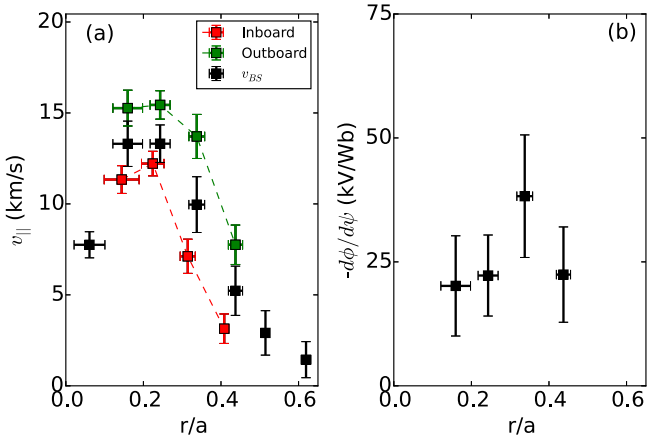

Figure 3. (a) Parallel flow velocity obtained from toroidal CHERS measurements for the QHS configuration at the inboard (red) and outboard (green) locations. Also plotted is the bootstrap component of the flow. (b) The flux surface constant, $-\frac{d\phi}{d\psi}$, obtained from the Pfirsch–Schlüter flows, using equation (1).

for both configurations is kept at 1 Tesla. Two gyrotrons were used to generate and heat the plasma through electron cyclotron heating (ECH) with a total injected power of 100 kW. Methane is used as the working gas for these experiments to improve the carbon signal for the spectroscopy.

The Pfirsch–Schlüter factor h, calculated by solving magnetic differential equations [10] at the measurement locations for these two configurations, is shown in figure 1(b). These values are weighted averaged along the sight-line within the beam width using a synthetic diagnostic model [11]. It can be seen that the Pfirsch–Schlüter factor has the opposite sign at inboard and outboard locations for the same flux surface (same r/a values, where r/a is the square root of the normalized toroidal flux), showing that the Pfirsch–Schlüter flows will be counter-streaming at these locations. The magnitude of the Pfirsch–Schlüter factor is nearly the same in both geometries for the same flux surface. Even though toroidal magnetic mirrors ($(n, m) = (4, 0)$ and $(8, 0)$ spectral components) are introduced for the Mirror configuration, because they are $m = 0$ they do not contribute to the calculation of h.

3. Experimental results

3.1. QHS geometry

The time evolution of the line-averaged electron density measured using an interferometer is shown in figure 2, along with radial profiles of the electron density and electron temperature measured using a Thomson scattering diagnostic. Carbon ion temperature measured using the CHERS diagnostic is also plotted in the figure, showing the nearly flat radial profile with $T_i \sim 50$ eV.

The parallel flow obtained from the measured toroidal flow is shown in figure 3. An asymmetry between the inboard/outboard measurements, as expected due to the counter-streaming Pfirsch–Schlüter flows, is clearly observed. It can be seen that the Pfirsch–Schlüter portion of the flow is adding to the bootstrap flow at the outboard locations and subtracting from the bootstrap flow at the inboard locations. The inboard/outboard asymmetry is such that the sign of the radial electric field is positive: the Pfirsch–Schlüter factor (figure 1(b)) and the sign of the Pfirsch–Schlüter flow are in opposite direction at any measurement location, making $E_r = -\frac{v_{PS}}{hB}$ positive.

The flux surface constants, $\frac{d\phi}{d\psi}$ and bootstrap flow (v_{BS}) are calculated from the two point measurements on a flux surface. The measurement locations are not exactly on the same flux surface (same r/a values) on both sides, as apparent from figure 3. An interpolation was used on one of the rows to calculate flows on the same flux surface on both sides. The bootstrap flow is shown as black points in figure 3. Here, three on-beam-axis measurements are also shown in black points as the Pfirsch–Schlüter factor at these locations is close to zero (see figure 1(b)). These three points are therefore showing the bootstrap flow. This value can now be directly compared with neoclassical bootstrap flow calculations. The flux surface constant, $-\frac{d\phi}{d\psi}$, calculated from the flow asymmetry is shown in figure 3(b).

3.2. Mirror geometry

Measurements were repeated for the Mirror configuration. For similar injected ECH power (100 kW) to that used in the QHS configuration, significantly lower core electron temperature (~0.8 keV compared to ~1.5 keV) is obtained for the Mirror geometry, as shown in figure 4. The line averaged electron density measured using the interferometer and the radial profile from the Thomson scattering diagnostic are similar to

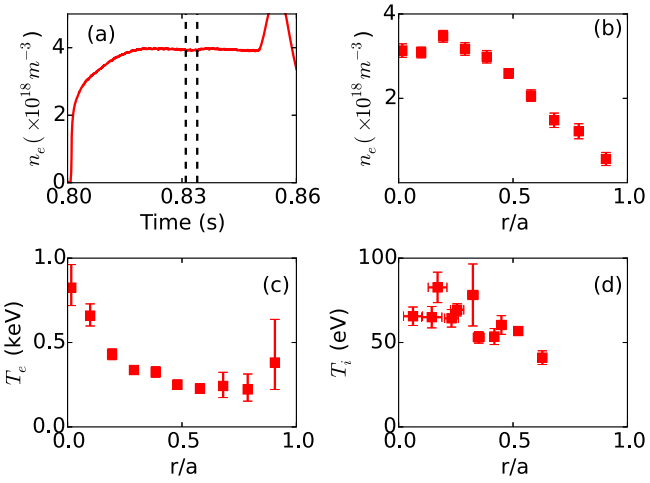

Figure 4. Discharge parameters for the Mirror configuration. Data are averaged over 19 similar discharges used for the flow and E_r analysis. Other details are similar to that in figure 2.

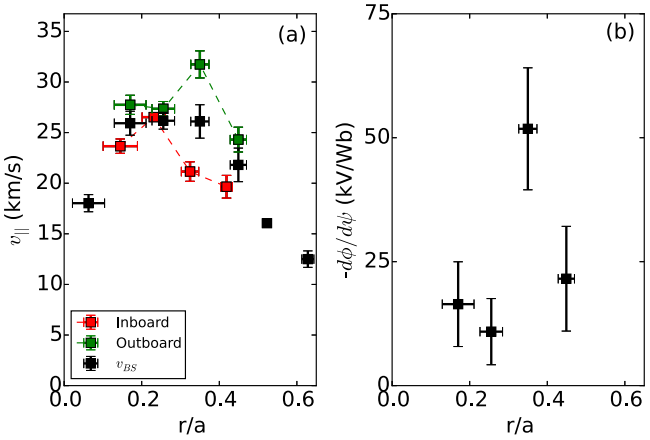

Figure 5. (a) Parallel flow velocity obtained from toroidal CHERS measurements for the Mirror configuration at the inboard (red) and outboard (green) locations. Also plotted is the bootstrap component of the flow. (b) The flux surface constant, $-\frac{d\phi}{d\psi}$, obtained from the Pfirsch–Schlüter flows, using equation (1).

those obtained for the QHS geometry. The ion temperature is low, as in the QHS configuration, and the profile is nearly flat.

The parallel flow for the Mirror geometry is shown in figure 5(a), along with the bootstrap flow calculated from the inboard/outboard asymmetry. The radial electric field, $-\frac{d\phi}{d\psi}$ obtained from the Pfirsch–Schlüter portion of the flow for the Mirror configuration is shown in figure 5(b).

4. Comparison of experiment to neoclassical calculations

Neoclassical calculations for this work are carried out using the PENTA code [12, 13]. Along with electron and ion temperatures and densities, the fractional abundance of carbon impurity calculated using a collisional radiative model from ADAS [14] and scaled to match carbon and hydrogen proportion in methane is also used in the calculation. The

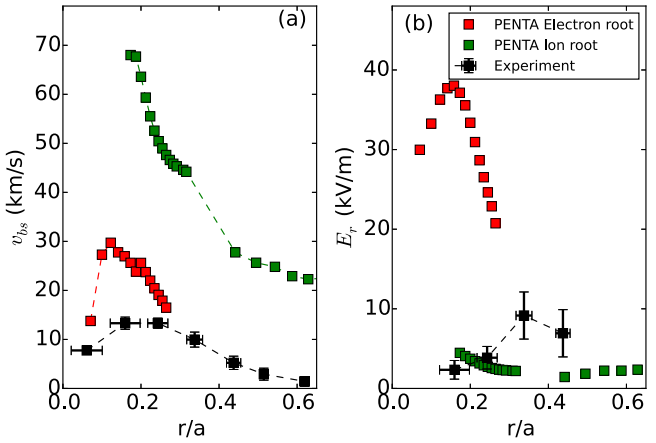

Figure 6. Neoclassical (red and green points) and experimental (black points with error bars) values of bootstrap flow (a) and E_r (b) for the QHS configuration. Red and green represent the electron-root and ion-root values respectively.

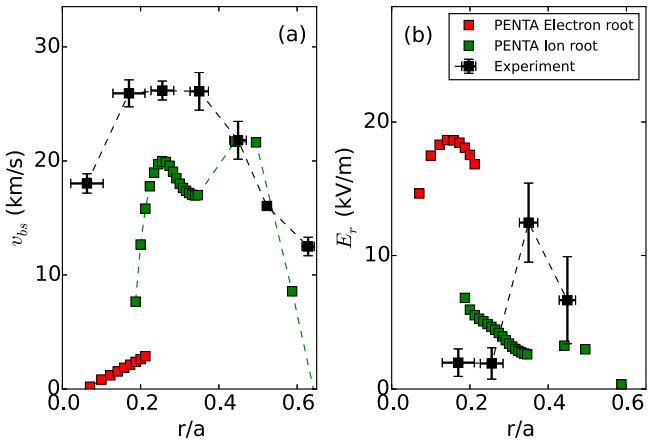

Figure 7. Neoclassical (red and green points) and experimental (black points with error bars) values of bootstrap flow (a) and E_r (b) for the Mirror configuration. Red and green represent the electron-root and ion-root values respectively.

neoclassical transport code PENTA uses a radial coordinate based on the toroidal flux. The measured radial electric field ($-\frac{d\phi}{d\psi}$), as shown in figures 3(b) and 5(b), are converted to the PENTA variable ($-\frac{d\phi}{dr_{\mathrm{PENTA}}}$) using the relation, $\psi = \pi r^2_{\mathrm{PENTA}} B_0$, where ψ and B_0 are toroidal magnetic flux and magnetic field strength respectively. The PENTA calculated ambipolar E_r and parallel flow profiles as a function of normalized minor radius for the experimental parameters are shown in figures 6 and 7 for QHS and Mirror configurations, respectively. The E_r and bootstrap flow obtained from the experiment are also plotted in these figures. The calculated neoclassical flows and electric field are much lower for the Mirror case for the same injected power.

It can be seen from figure 6 that even though the radial electric field is slightly higher than the previously obtained value of $\sim$5 kV m^{-1} [9], the large discrepancy between the measurement and the code calculation, as reported in those previous experiments, still exists for the QHS configuration. The experiment could not detect either the large electron-root

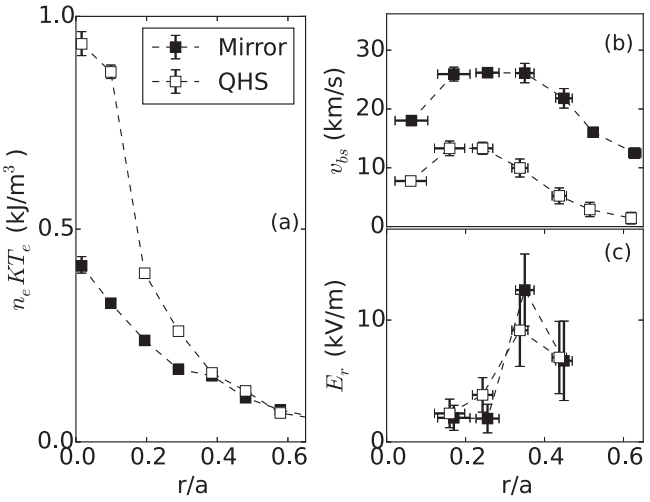

Figure 8. Comparison of the electron pressure profiles (a), experimental bootstrap flows (b) and experimental E_r (c) for QHS (open squares) and Mirror (filled squares) configurations.

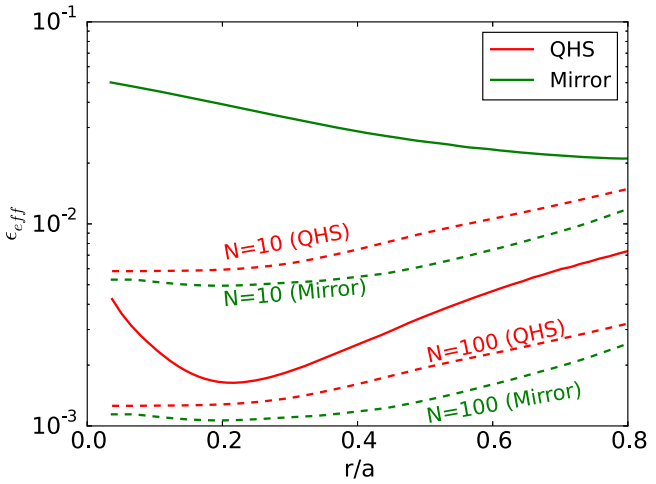

Figure 9. Effective helical ripple for QHS and Mirror configurations (solid lines) and the RHS of equation (2) calculated for $N = 10$ and $N = 100$ in dotted lines.

positive radial electric field at the core or the large ion-root parallel flows calculated by the PENTA code. The inconsistency in this comparison is that, while the electric field values agree with the ion-root solution, the bootstrap flow is close to the electron-root solution. However, both E_r and the bootstrap flows in the Mirror configuration are close to the ion root solution near the core (see figure 7), a consistency that is missing in the QHS case. The agreement with the neoclassical calculation is better for the configuration in which neoclassical transport is increased compared to the neoclassically optimized quasi-symmetric configuration.

5. Discussions

The bootstrap flow and the radial electric field for the QHS and the Mirror geometries are compared in figure 8. The electron pressure profile for both geometries are also shown for comparison. It can be seen that even though the QHS case had significantly higher electron pressure and pressure gradients, the flows are lower by a factor of two compared to the configuration in which the quasi-symmetry is degraded. This observation is contrary to our expectation of reduced neoclassical flow damping in the QHS, as shown in previous experiments [8]. The radial electric field is similar in both cases. The reason for this slower rotation in the QHS case is not understood at present.

We now examine whether the quasi-symmetric nature of the QHS configuration explains the discrepancy between the experiment and neoclassical calculations. The effective helical ripple, $\epsilon_{\rm eff}$ [15], is a measure of transport in the low collisionality '$1/\nu$ regime' through the relation, $D_{1/\nu} \sim \epsilon_{\rm eff}^{3/2} v_d^2/\nu$ where $D_{1/\nu}$ is the diffusion coefficient, v_d is the drift velocity and ν is the collision frequency. The $\epsilon_{\rm eff}$ for the QHS configuration is about two orders of magnitude lower than that of the Mirror configuration, as shown in figure 9. However, this QHS $\epsilon_{\rm eff}$ is still many orders of magnitude higher than that of an axi-symmetric tokamak. Therefore, it is not obvious that the QHS device can behave similar to an intrinsically ambipolar device like an ideal tokamak, where flows and electric field are determined by non-neoclassical properties. The extent of deviation of a magnetic configuration from an ideal quasi-symmetric configuration determines whether the flows and electric fields are governed by neoclassical or non-neoclassical processes.

One such calculation, following Helander and Simakov [4] is shown below. Assuming low-collisionality ions, the non ambipolar current exceeds that driven by Reynolds stress, if

$$\epsilon_{\rm eff} > \left(\frac{L}{N\lambda_{\rm MFP}}\right)^{2/3}, \qquad (2)$$

where $\epsilon_{\rm eff}$ is the effective helical ripple, L is a macroscopic scale length (average minor radius of the plasma is used here), $\lambda_{\rm MFP}$ is the ion collision mean free path, N is a number greater than 1. Shown in figure 9 is the effective ripple for Mirror and QHS in solid lines along with the right hand side of equation (2) calculated for two values of N, 10 and 100. It is apparent that, the condition given in equation (2) is always satisfied for the Mirror geometry, showing that neoclassical processes determine the radial electric field and flows. However, for the QHS case non-neoclassical processes dominate at lower values of N and neoclassical processes dominate at much higher values of N.

Another way to look at this condition is to calculate the radial width over which non-neoclassical processes dominate, $\Delta r = N\rho_i = \frac{L}{\epsilon_{\rm eff}^{3/2}\lambda_{\rm MFP}}\rho_i$, where ρ_i is the ion gyro radius. This 'critical width' is plotted for QHS and Mirror geometries as a function of minor radius, in figure 10. Also shown is the average radius of the plasma. For QHS, the critical width becomes comparable or greater than the minor radius of the plasma near the core, but for the Mirror geometry, it is always much less than the plasma minor radius. Therefore, near the core of the QHS plasma, flows and E_r may be determined by non-neoclassical processes. A disagreement with neoclassical calculations of E_r and flows is therefore expected for the QHS plasma near the core region. It has to be noted that this analysis assumes ions in the $1/\nu$ regime, whereas in our

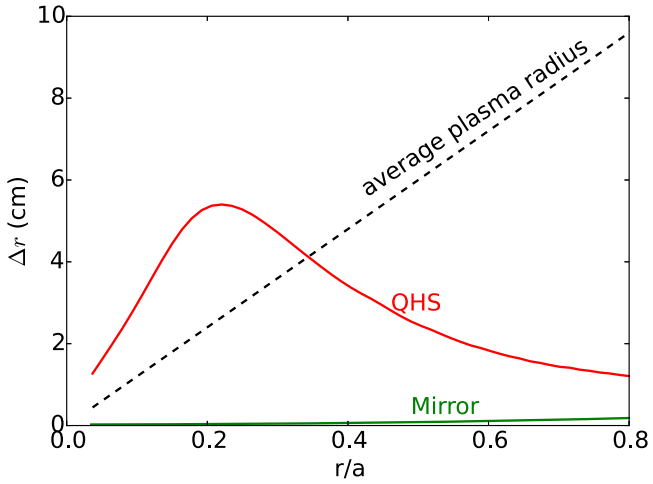

Figure 10. The 'critical width' estimated for QHS (red) and Mirror (green) configurations. Also plotted is the averaged plasma radius.

experiment they are in plateau regime. This assumption results in overprediction of the neoclassical non ambipolar current, making the contribution of non-neoclassical processes to dominate more.

6. Summary

Counter-streaming Pfirsch–Schlüter flows have been observed in the HSX stellarator. Measurements are made in quasi-symmetric and in a configuration with quasi-symmetry degraded, with similar injected heating power. Significantly lower mean ion flows have been observed in the quasi-symmetric configuration. Measurements for the Mirror configuration is in better agreement with neoclassical calculations. The reason why there is lower bootstrap flow in the quasi-symmetric configuration and a large discrepancy with the neoclassical flows is not well understood at present, but a preliminary analysis indicate that the flows and E_r near the core of the quasi-symmetric geometry may be governed by non-neoclassical processes.

Acknowledgments

The authors would like to thank F S B Anderson and K Likin for help with machine operation. The material presented in this paper is based upon work supported by the US Department of Energy, Office of Science, Office of Fusion Energy Science under award number DE-FG02-93ER54222. Data for figures included in this publication are available for access at http://hsx.wisc.edu/HSXPublicationData.

ORCID iDs

S T A Kumar https://orcid.org/0000-0002-6444-5178

References

[1] Baldzuhn J, Kick M, Maassberg H and The W7-AS Team 1998 Measurement and calculation of the radial electric field in the stellarator W7-AS *Plasma Phys. Control. Fusion* **40** 967
[2] Yokoyama M, Wakasa A, Murakami S, Watanabe K Y, Satake S, Nishimura S, Sugama H, Nakajima N, Funaba H and Nakamura Y 2010 Role of neoclassical transport and radial electric field in LHD plasmas *Fusion Sci. Technol.* **58** 269–76
[3] Gutiérrez-Tapia C, Martinell J J, Lõpez-Bruna D and Melnikov A V 2015 Neoclassical modeling of the radial electric field and comparison with measurements in the TJ-II stellarator *J. Phys.: Conf. Ser.* **591** 012011
[4] Helander P and Simakov A N 2008 Intrinsic ambipolarity and rotation in stellarators *Phys. Rev. Lett.* **101** 145003
[5] Calvo I, Parra F I, Velasco J L and Alonso J A 2013 Stellarators close to quasisymmetry *Plasma Phys. Control. Fusion* **55** 125014
[6] Anderson D T *et al* 2006 Overview of recent results from HSX *Fusion Sci. Technol.* **50** 171
[7] Canik J M, Anderson D T, Anderson F S B, Likin K M, Talmadge J N and Zhai K 2007 Experimental demonstration of improved neoclassical transport with quasihelical symmetry *Phys. Rev. Lett.* **98** 085002
[8] Gerhardt S P, Talmadge J N, Canik J M and Anderson D T 2005 Measurements and modeling of plasma flow damping in the helically symmetric experiment *Phys. Plasmas* **12** 056116
[9] Briesemeister A, Zhai K, Anderson D T, Anderson F S B and Talmadge J N 2013 Comparison of the flows and radial electric field in the HSX stellarator to neoclassical calculations *Plasma Phys. Control. Fusion* **55** 014002
[10] Kumar S T A, Talmadge J N, Dobbins T J, Anderson F S B, Likin K M and Anderson D T 2017 Determination of radial electric field from Pfirsch–Schlüter flows in the hsx stellarator *Nucl. Fusion* **57** 036030
[11] Dobbins T J, Kumar S T A and Anderson D T 2016 A synthetic diagnostic for beam emission spectroscopy in the helically symmetric experiment stellarator *Rev. Sci. Instrum.* **87** 11D413
[12] Spong D A 2005 Generation and damping of neoclassical plasma flows in stellarators *Phys. Plasmas* **12** 056114
[13] Lore J, Guttenfelder W, Briesemeister A, Anderson D T, Anderson F S B, Deng C B, Likin K M, Spong D A, Talmadge J N and Zhai K 2010 Internal electron transport barrier due to neoclassical ambipolarity in the helically symmetric experiment *Phys. Plasmas* **17** 056101
[14] Summers H P 2004 The ADAS User Manual, version 2.6
[15] Nemov V V, Kasilov S V, Kernbichler W and Heyn M F 1999 Evaluation of $1/\nu$ neoclassical transport in stellarators *Phys. Plasmas* **6** 4622–32